Available online at www.sciencedirect.com
ScienceDirect
Polymer 48 (2007) 4751–4764
polymer
www.elsevier.com/locate/polymer

Low electrical conductivity threshold and crystalline morphology of single-walled carbon nanotubes – high density polyethylene nanocomposites characterized by SEM, Raman spectroscopy and AFM

Keesu Jeon [a], Lloyd Lumata [b], Takahisa Tokumoto [b], Eden Steven [b], James Brooks [b], Rufina G. Alamo [a,*]

[a] *FAMU/FSU College of Engineering, Department of Chemical and Biomedical Engineering, 2525 Pottsdamer St, Tallahassee, FL 32310-6046, USA*
[b] *National High Magnetic Field Laboratory, 1800 E. Paul Dirac Dr. Tallahassee, FL 32310-6046, USA*

Received 16 April 2007; received in revised form 23 May 2007; accepted 31 May 2007
Available online 8 June 2007

Abstract

The electrical conductivities (σ) of nanocomposites of single-walled carbon nanotubes (SWCNTs) and high density polyethylene (HDPE) have been studied for a large number of nanocomposites prepared in a SWCNT concentration range between 0.02 and 8 wt%. The values of σ obey a percolation power law with an SWCNT concentration threshold, $p_c = 0.13$ wt%, the lowest yet obtained for any kind of carbon–polyethylene nanocomposites. Improved electrical conductivities attest to an effective dispersion of SWCNT in the polyethylene matrix, enabled by the fast quenching crystallization process used in the preparation of these nanocomposites. Characterization by scanning electron microscopy (SEM) and Raman spectroscopy consistently points to a uniform dispersion of separate small SWCNT bundles at concentrations near p_c and increased nanotube clustering at higher concentrations. Near p_c, high activation energies and geometries of long isolated rods suggest that electron transport occurs by activated electron hopping between nanotubes that are close to each other but still geometrically separate. The degree of SWCNT clustering given by Raman spectroscopy and the barrier energy for electrical conductivity are highly correlated. The nanotubes act as nucleants in the crystallization of the polyethylene matrix, and change the type of supermolecular aggregates from spherulites to axialitic-like objects. The size of crystal aggregates decreases with SWCNT loading, however, in reference to the unfilled polyethylene, the three-dimensional growth geometry extracted from the Avrami exponents remains unchanged up to 2 wt%. Consistency between SEM, Raman and electrical transport behavior suggests that the electrical conductivity is dominated by dispersion and the geometry of the SWCNT in the nanocomposites and not by changes or lack thereof in the HDPE semicrystalline structure.

Keywords: SWCNT; Polyethylene nanocomposites; Crystallization

1. Introduction

Carbon nanotubes (CNTs) have attracted considerable attention due to their extraordinary mechanical, electrical, optical, and thermal properties [1,2]. Especially, the high aspect ratio (up to ~1000) of CNTs renders enhanced material properties at very low CNT concentration in CNT-based polymer nanocomposites. Compared to carbon black and other reinforcements, the shear and tensile strengths, and modulus of CNT composites increase significantly at much lower load levels. Conversely, except in isolated cases [3], toughness and elongation are found to decrease in reference to the pure resin. In addition to property strength at relatively low loads, the mechanical, electrical and thermal properties of a large variety of single-walled carbon nanotube (SWCNT) nanocomposites improve with increased debundling and uniformity of the dispersion in the polymer matrix [2]. Consequently, most

* Corresponding author.
E-mail addresses: keesu@eng.fsu.edu (K. Jeon), brooks@magnet.fsu.edu (J. Brooks), alamo@eng.fsu.edu (R.G. Alamo).

0032-3861/$ - see front matter © 2007 Elsevier Ltd. All rights reserved.
doi:10.1016/j.polymer.2007.05.078

methods for preparation of nanocomposites have focused on improving nanotube dispersion by some mechanism that minimizes or prevents the high driving force of the CNT to aggregate due to strong C–C van der Waals forces. These methods include solution sonication, improvement of solvent quality allowing more efficient debundling, use of surfactants, CNT surface modification, and CNT length reduction.

Dispersing SWCNTs in a polyethylene (PE) matrix in a solution blending method without the aid of surfactants relies on the interaction between the SWCNTs, PE and solvent. The choice of solvent is a key factor to circumvent the strong van der Waals interactions between SWCNTs, and to obtain well-dispersed SWCNTs in the PE matrix. Among many solvents studied, 1,2-dichlorobenzene (1,2-DCB) is one of the best organic solvents to disperse CNT in PE. In addition to a high solubility for CNT [4], it has been postulated that sono-chemical changes in 1,2-DCB structure during sonication aid with the nanotube debundling process [5].

Polyethylenes are the most affordable polyolefin-based thermoplastics. In light of the large spectrum of applications, improvements and technical breakthroughs in these materials can yield significant economic impact. Our purpose here is to show that a carefully controlled fast crystallization from a dilute solution of a SWCNT–HDPE mixture maintains the uniformity of the CNT dispersion in the solvent, thus providing HDPE nanocomposites with improved electrical conductivities. The SWCNT dispersion in the HDPE matrix is determined using standard optical microscopy (OM), scanning electron microscopy (SEM), as well as charge-contrast SEM imaging and Raman spectroscopy. A basically invisible crystalline structure in charge-contrast SEM provides information of the dispersion and organization of the SWCNTs at relatively large depth scales [6]. These results are further compared with predictions made by simple percolation models for isotropic dispersions of rod-like particles [7,8].

Previous electrical conductivity studies of HDPE–CNT nanocomposites investigated concentrations above ~1 wt% [9], consequently, the percolation thresholds reported are well above this value. These earlier reports involved PE nanocomposites with multiwalled carbon nanotubes (MWCNTs) [10–12], or solution [10] or melt blending [12] carbon black (CB) polyethylene nanocomposites. Only in one recent report electrical conductivities were given for HDPE–SWCNT nanocomposites for concentrations above ~1 wt% [13].

In the present work we prepared nanocomposites of SWCNTs and linear polyethylene (HDPE) via fast crystallization from 1,2-DCB solutions. This process has been shown to be effective as a way to entrap the CNTs within the semicrystalline structure while preserving the uniform CNT dispersion in solution [14]. In particular, SWCNT–HDPE nanocomposites with SWCNT concentrations below and above 1 wt% were prepared, to enable a detailed determination of the percolation threshold for electrical conductivity. The dispersion and geometries of SWCNT bundles below and above the threshold concentrations are inferred from SEM.

Studies of the crystallization behavior and morphology of flow-oriented and quiescent melts of SWCNT-based polyethylene nanocomposites have appeared recently [3,9,14–17]. Highly structured composites result from the strong nucleation effect of oriented SWCNTs on PE crystallization. In reference to neat polyethylene, its CNT nanocomposites present shorter crystallization half-times and smaller lamellar aggregates, usually non-spherulitic. In the present work, the nucleation activity of the filler is studied at much lower SWCNT concentrations than in previous work, and over a wider SWCNT concentration range, from 0.02 to 8 wt%. Changes in the supermolecular morphology by the addition of nanotubes are studied by AFM.

2. Experimental methods

2.1. Materials and nanocomposite preparation

An industrial grade high density polyethylene (Sclair HDPE) was chosen as the nanocomposite matrix. The molecular weight measured by standard gel permeation chromatography is $M_w = 53{,}600$ g/mol and $M_w/M_n = 2.35$. Purified SWCNTs HiPco were purchased from Carbon Nanotechnologies Inc. and used as-received.

SWCNT–HDPE nanocomposites were prepared by fast crystallization from dilute solution [18]. A measured amount of SWCNTs was first added to 1,2-dichlorobenzene (1,2-DCB, Aldrich), and ultrasonicated for 3 h using a tip sonicator (Sonicator 3000, Misonix) operating at a power of 36–45 W and frequency of 20 kHz. The temperature of the solution increased gradually during sonication, reaching a value of ~130 °C after 180 min. In a separate vessel, polyethylene was dissolved in 1,2-DCB at ~130 °C stirring the solution for 20 min. The hot sonicated SWCNT solution was added to the HDPE solution at ~130 °C and thoroughly mixed with a Teflon magnetic stirrer for an additional 20 min at this temperature. Finally, the hot solution was quickly poured into methanol at 6 °C (1:5 v/v) and kept at 4 °C overnight. The supernatant liquid was transparent, and the precipitate lacked black lump aggregates, indicating that the SWCNTs were incorporated in the HDPE matrix. The precipitate was filtered using porcelain filters with 10–15 μm pore sizes, washed with methanol, and dried overnight in a vacuum oven at ~90 °C. Nanocomposites were prepared with the following concentrations of SWCNT in HDPE: 0.02, 0.05, 0.07, 0.1, 0.15, 0.2, 0.25, 0.3, 0.35, 0.4, 0.5, 0.65, 0.8, 2, and 8 wt%. The concentrations of SWCNT in 1,2-DCB used to formulate nanocomposites with less than 0.8 wt% SWCNT in HDPE were all below the estimated room temperature solubility (95 mg/L) [4], those used to prepare 2 and 8 wt% SWCNT–HDPE samples were higher than this value. HDPE concentrations in the mixed 1,2-DCB solution were in the range of 3–4 g/L for the nanocomposites with ≥0.1 wt% SWCNT, and 6–13 g/L for SWCNT concentrations lower than 0.1 wt% in PE. To obtain a reference material free of SWCNTs, the original HDPE was dissolved in 1,2-DCB at ~130 °C and precipitated in methanol at 6 °C, followed by the same washing and drying procedures. This sample was used to compare properties of filled and unfilled HDPE under the same solvent treatment.

2.2. Techniques

The macroscopic dispersion of SWCNTs was first investigated by optical transmission microscopy. After sonication and prior to mixing with the HDPE solution, a few drops of SWCNT solution in 1,2-DCB were poured on a cover glass and dried at room temperature. Optical micrographs were obtained at room temperature using an Olympus BH-2 microscope connected with an Olympus DP12 digital camera.

The dispersion of SWCNTs, prior and after mixing with HDPE, was characterized in more detail by field-emission scanning electron microscopy (FE-SEM, JEOL JSM-7301F). Two types of samples were imaged. One type was SWCNTs deposited and dried on cover glass and a second type comprised fractured surfaces of the same nanocomposite films used for electrical conductivity measurements. The films were lightly indented with a razor blade, immersed in liquid nitrogen and fractured while frozen in the liquid nitrogen. These surfaces were coated with Au/Pt and imaged at 5 kV. In addition, uncoated fractured surfaces from the same nanocomposites were imaged using charge-contrast imaging at 10 kV [6]. The SEM images were collected from a minimum of five different locations of each specimen.

The electrical conductivity was measured in molded plaques with dimensions 6 mm × 3 mm × 0.45 mm that were slowly cooled from the melt to room temperature at ~2 °C/min. Direct-current (DC) conductivity measurements using a four-point contact method eliminated contact-resistance effects. The four contacts were made in line across the 3 mm length of the samples using 25 μm gold wires and carbon paste. The current was supplied using a Keithley 6221 DC source; the voltage was measured with a Keithley 2182A nanovoltmeter (for samples below about 100 MΩ), or with a Keithley 6517A electrometer (for samples greater than 100 MΩ). For sample resistances above 50 GΩ, leakage currents in the circuitry became significant.

For temperature dependent measurements samples were placed in a sealed probe on a copper sample holder with a platinum thermometer. The probe was evacuated and helium was used as the exchange gas. The temperature dependent resistivity could then be determined by cooling the samples to liquid nitrogen temperature (typically for lower resistance samples with 0.24 wt% or more). Higher resistance samples (with 0.2 wt% or less) were measured at room temperature and above by warming the sealed probe in a glycerol or water thermal bath.

Crystallization and melting properties of the reference HDPE and the nanocomposites were investigated using a Perkin–Elmer differential scanning calorimeter DSC-7 under nitrogen flow. Small pieces (3 ± 0.2 mg) cut from molded films were encapsulated in aluminum pans, and underwent subsequent cooling and heating scans between 50 °C and 180 °C at 10 °C/min. As a test of uniformity of the SWCNT distribution in the HDPE matrix, five different sample pans were analyzed for each nanocomposite and for the reference HDPE. The specific heat flow from the corresponding crystallization and melting peaks (W/g) was corrected for the mass of HDPE in the nanocomposite. The corrected heats of fusion were used to determine the degrees of crystallinity of the nanocomposites, based on a value of 290 J/g for the fully crystalline polyethylene [19]. The instrument's temperature and heat flow were calibrated with indium as a standard.

Films for atomic force microscopy (AFM) imaging were prepared by casting ~3 drops of the SWCNT–HDPE hot solution in 1,2-DCB on cover glasses prior to their precipitation in methanol. The solvent was allowed to evaporate at room temperature. The film thicknesses calculated from the areas and weights of the films were ~4 μm for the HDPE film and ~2 μm for the nanocomposites. The films were melted at 180 °C for 3 min, cooled down to 120 °C at 40 °C/min, and held at this temperature for 1 h (nanocomposites) or 16 h (HDPE), for isothermal crystallization. An environmental JEOL 4210 scanning probe microscope was used for AFM imaging with Olympus single side coated silicon cantilevers (spring constants of ~40 N/m and a tip radius of less than 10 nm) at a resonant frequency of ~300 kHz. Topographic and phase images were simultaneously collected under ambient conditions in non-contact AC mode at 256 × 256 standard resolution.

Raman spectra were obtained using a Renishaw Invia Raman microscope in the back-scattering configuration with a 50× objective. The size of the laser spot on the surface of the sample was less than 1 μm in diameter. The 785 nm (1.58 eV) line was used for excitation with a laser power of 0.5 mW. As a test of uniformity of dispersion of SWCNT in the matrix, Raman spectra were collected at five different positions of the as-received SWCNTs, and the molded nanocomposite films.

3. Results and discussion

3.1. Dispersion of SWCNTs

The dispersion of SWCNTs in the solvent, and within the HDPE matrix, was investigated by OM, SEM and Raman spectroscopy. Optical micrographs (not shown) of sonicated SWCNTs after 1,2-DCB evaporation, for SWCNT concentrations below 80 mg/L, did not show any sign of SWCNT bulk aggregation. This was inferred by the lack of any visible black features associated with carbon nanotubes at the micron scale level. This range of concentration was used to formulate nanocomposites up to 1 wt% SWCNT. In contrast, concentrations >80 mg/L used in the preparation of PE nanocomposites with higher SWCNT contents, displayed black visible aggregates in length scales of 50–100 μm. If one assumes that the morphology of dry SWCNTs on the glass substrate is representative of the level of dispersion of the nanotubes in the suspension, then the micrographs indicate a uniform dispersion of the nanotubes in the low concentrated solutions and a tendency to agglomerate as the nanotube concentration increases above 80 mg/L. It turns that this concentration dependence is consistent with a room temperature solubility value of 95 mg/L given for SWCNT in 1,2-DCB [4].

More dramatic evidence of the highly uniform dispersion achieved for concentrations of SWCNT in 1,2-DCB <50 mg/L is shown in the SEM images of Fig. 1. The concentrations shown correspond to those used to formulate 0.15 wt% (a) and 0.4 wt% (b) SWCNT–HDPE nanocomposites, respectively. On a submicron scale, we observe nanotubes quite uniformly distributed in both images. The images display isolated, relatively straight nanotube bundles, with an average length of 300 ± 130 nm and diameter of 7.4 ± 1.8 nm, given by the histograms of Fig. 1c and d, respectively. These histograms are derived from ~200 data of the more diluted sample. The average length of the nanotubes is significantly shorter than the presumed ~1 μm original length [20] suggesting that the nanotubes undergo scission during sonication. The observed lump aggregates most probably correspond to remains of hard metallic catalyst particles or to graphitic impurities that are present in the original SWCNTs from the synthetic process. Other sources such as solvent impurities or tube rebundling after solvent evaporation cannot be ruled out.

Stable solutions of well-dispersed SWCNT at 130 °C were poured into preheated and stirred polyethylene solutions at the same temperature in order to obtain a uniform dispersion of the nanotubes within the polymer random coil. It is presumed that on rapid cooling of this solution, nucleation of polyethylene crystallites on the surface of the nanotubes facilitates pinning and entrapment of the SWCNT within the semicrystalline matrix. Polyethylene nucleation and growth from the walls of debundled nanotubes help to overcome the strong van der Waals carbon–carbon interactions responsible for the SWCNTs tendency to cluster, and thus, help to preserve the original nanotube dispersion in the sonicated solution. In other words, growth of the semicrystalline structure from the nanotubes acts as a barrier to prevent their clustering.

Figs. 2 and 3 show SEM images of fractured surfaces of films that were slowly cooled from the melt at ~2 °C/min. Fig. 2 displays standard images of coated surfaces for nanocomposites with SWCNT concentrations of 0.8, 2, and 8 wt% at two different magnifications. At a concentration of 8 wt% a continuous network of highly interconnected nanotubes can be distinguished from crystalline lamellae. The network appears homogeneously distributed in the polymer matrix. At this relatively high concentration, PE lamellar crystallites are short and poorly developed. The number of SWCNTs observed in the micrographs decreases dramatically with decreasing concentration of nanotubes in the nanocomposite, and are rarely observed at concentrations below 0.8 wt%. The arrows in the SEM image of 0.8 wt% nanocomposite

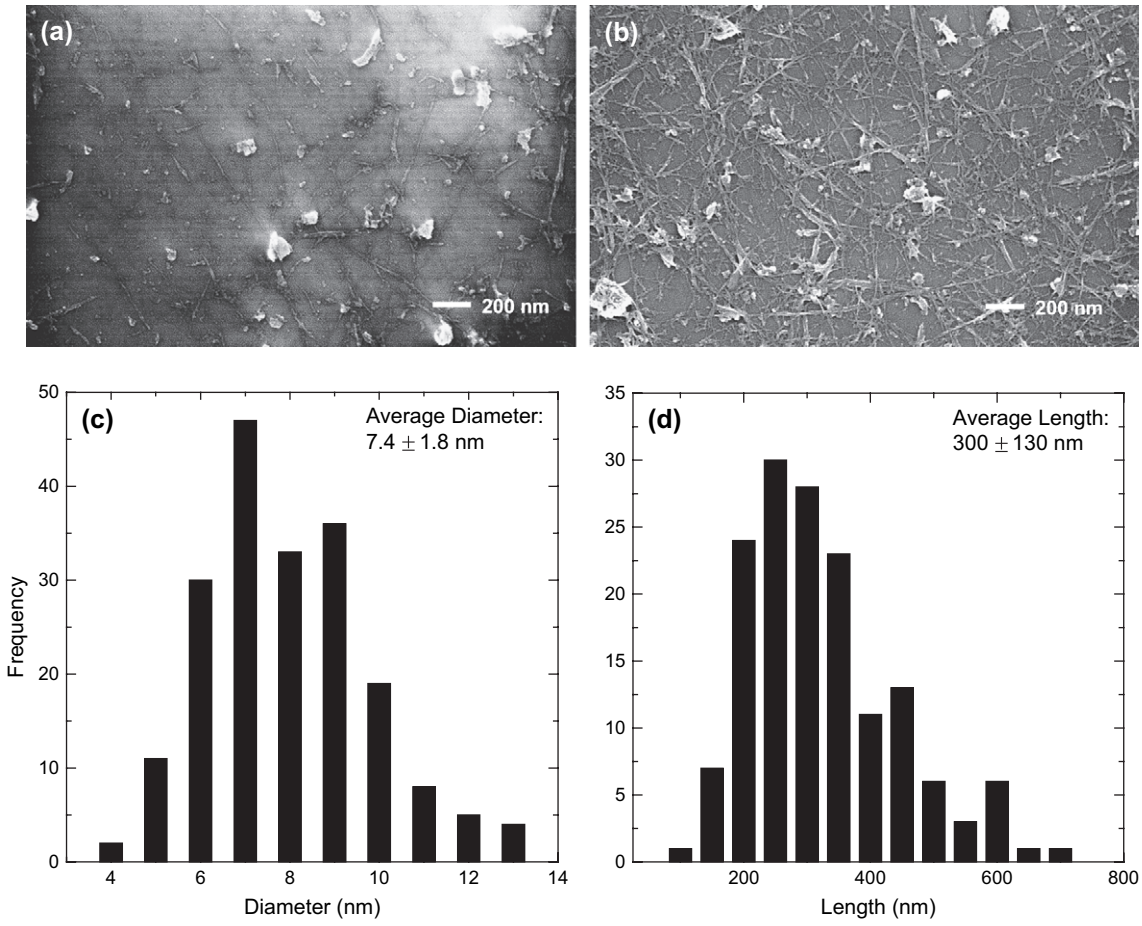

Fig. 1. SEM images of dried and coated SWCNTs on cover glasses from sonicated solutions in 1,2-DCB. (a) ~8 mg/L, (b) ~21 mg/L. These solutions were used to fabricate 0.15 and 0.4 wt% SWCNT–HDPE nanocomposites, respectively. (c) and (d) Histograms of nanotube sizes from micrographs similar to (a).

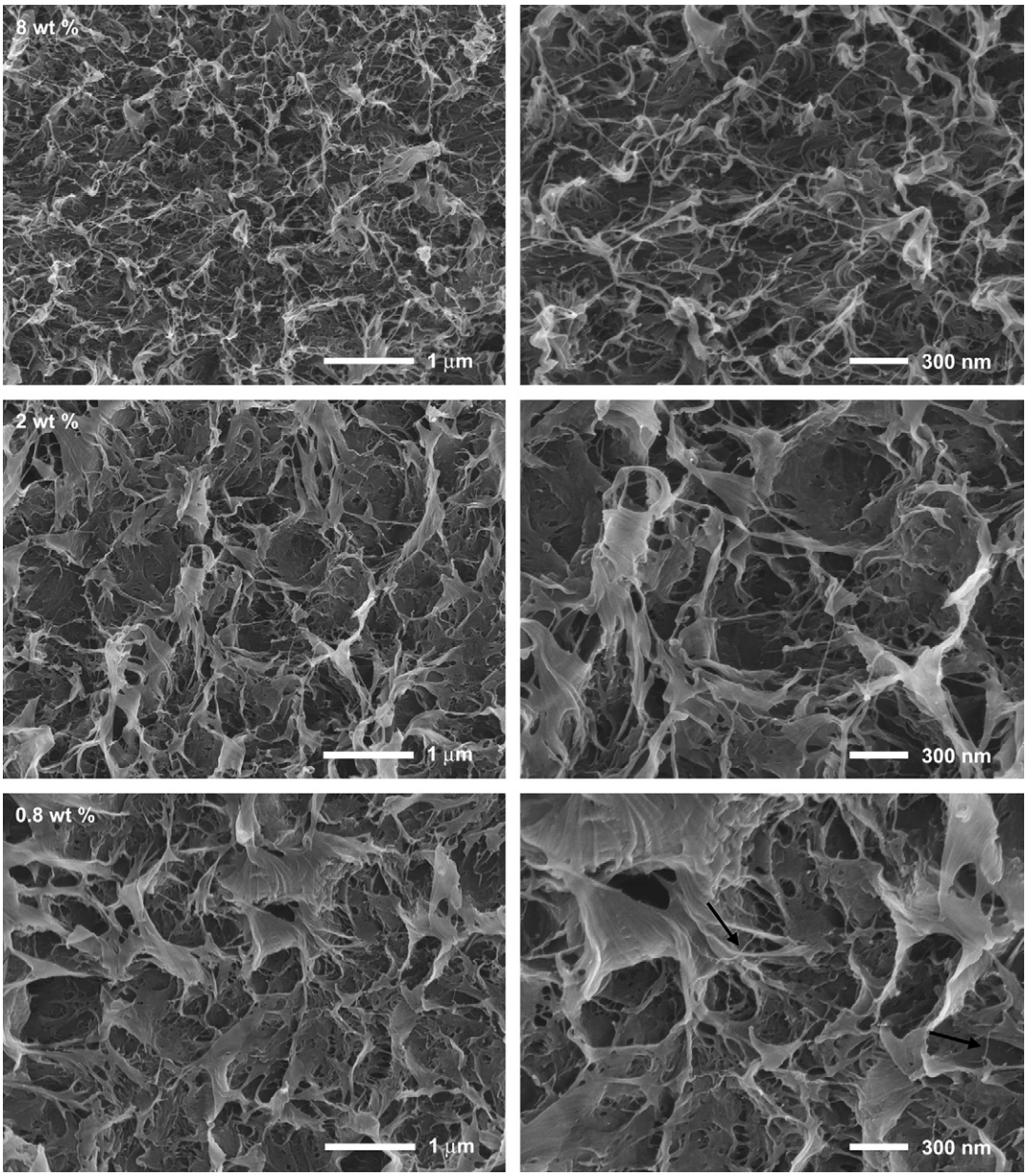

Fig. 2. SEM images of coated fractured surfaces corresponding to 0.8, 2, and 8 wt% SWCNT–HDPE nanocomposites. Two magnifications are shown. Isolated ropes connecting crystallites are distinguished in 8 wt% nanocomposites, and indicated by arrows in the 0.8 wt% sample.

point towards isolated SWCNTs connecting crystalline lamellae. On the other hand, the crystalline lamellae appear wider and better developed as the concentration of SWNT decreases. Lamellar stacks, as those required for supermolecular structures of the spherulitic or axialitic type are observed at SWCNT concentrations $\leq \sim 1$ wt%, this is a feature that correlates with volume limitations for crystal growth within the PE matrix as the content of CNTs increases.

Standard SEM images from coated surfaces only provide an image of a cross section of the three-dimensional arrangement of the CNTs, a limitation in the process of imaging the SWCNT dispersion within the crystalline polymer. Furthermore, in a crystalline matrix, lamellar crystals that protrude from the fractured surface provide additional contrast and features that, in many cases, are difficult to distinguish from those corresponding to the CNT filler, as seen in the images of Fig. 2. For example, any SWCNT lying below flat-on lamellae will be invisible in the SEM images. To improve contrast visualizing CNTs in a polymeric nanocomposite, SEM in the charge-contrast imaging mode has been proposed as a method to provide images of the CNT dispersion up to ~ 2 μm from the nanocomposite surface [6,21]. According to this technique, SEM images are taken from untreated surfaces, operating at a higher voltage than the usual 5 kV when imaging coated surfaces. Contrast between the filler and the polymer matrix in these images is described as a result of accumulation of back-scattered secondary electrons at the location of the SWCNT. A higher charge density occurs at these locations during charge transport between the conductive fillers and the insulating matrix [6].

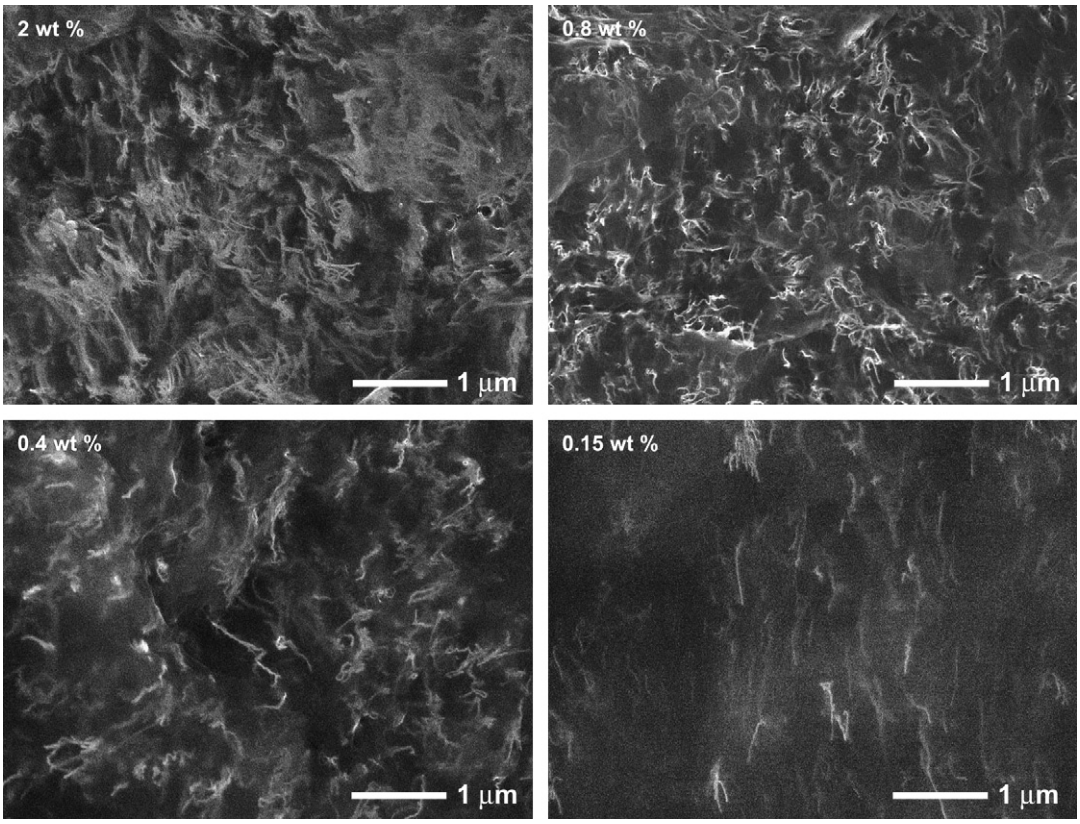

Fig. 3. Charge-contrast SEM images of uncoated fractured surfaces of the same SWCNT–HDPE nanocomposites with concentrations of 0.15, 0.4, 0.8, and 2 wt%. The SWCNT are preferentially observed in these images.

In light of the above, SEM images in the uncoated, charge-contrast mode were obtained from SWCNT–HDPE nanocomposites in a filler concentration range between 2 and 0.15 wt%. Representative images are given in Fig. 3. The applied voltage of 10 kV allows a ''pseudo'' three-dimensional image of the dispersion of CNTs at a penetration depth of ~1 μm. The number and characteristics of the SWCNTs dispersed among the matrix are better differentiated in these images. Charge contrast also allows visualizing the dispersion of SWCNTs in nanocomposites with concentrations as low as 0.15 wt%, while it was not possible to identify nanotubes in Fig. 2 for concentrations below 0.8 wt%. At the lowest concentration, fairly straight and some bent nanotubes are observed; brightness differences between them reflect the placement of nanotubes at different depths from the surface. The presence of multiple isolated ropes at the lowest concentration (0.15 wt%) suggests that a continuous network of overlapping nanotubes is not yet formed. The characteristics of this network are more readily apparent in the images of 0.8 and 2 wt%. Note that concentrations of nanotubes below 0.15 wt% could not be imaged due to common over-charging of the insulating matrix; thus, we can only predict that for concentrations at and below the electrical conductivity percolation limit (~0.13 wt% as discussed below), the dispersion of SWCNTs will follow the characteristics of the 0.15 wt% image at a higher dilution, i.e., primarily isolated nanotube ropes with rod-like appearance within the semicrystalline matrix.

The dispersion of SWCNTs in the HDPE matrix was also characterized by analyzing the changes in intensity of Raman bands corresponding to radial breathing modes (RBM) associated with isolated and bundled CNTs. This is the region of the Raman spectrum between 100 and 400 cm^{-1}, which is sensitive to differences in nanotube chirality and/or nanotube diameters. The population of nanotubes with different chiralities could be identified in reference to theoretical predictions, by systematically changing the wavelength of the excitation source [22]. It has been shown that a single excitation at 785 nm is quite useful to establish differences between bundled and isolated nanotubes [23]. The major difference at this excitation is the absence of the (10,2) RBM at 266 cm^{-1}, the so-called ''roping peak'', in the spectra of isolated tubes. Changes in the intensity of this peak relative to other RBM present in both isolated and bundled nanotubes give a qualitative estimation of the state of SWCNT aggregation. For example, the Raman spectra shown in Fig. 4 for the ''as-received'' SWCNTs and the HDPE nanocomposites show a prominent (12,1) RBM at 232 cm^{-1} in both the bundled ''as-received'' SWCNT and in the nanocomposites, while a low intensity of the 266 cm^{-1} mode for the lowest SWCNT concentrations indicates that only at these low concentrations the nanotubes are at the highest degree of isolation. The intensity of the 266 cm^{-1} mode increases with concentration of SWCNTs following the expected increase in bundle size, and has the highest value for the ''as-received'' nanotubes.

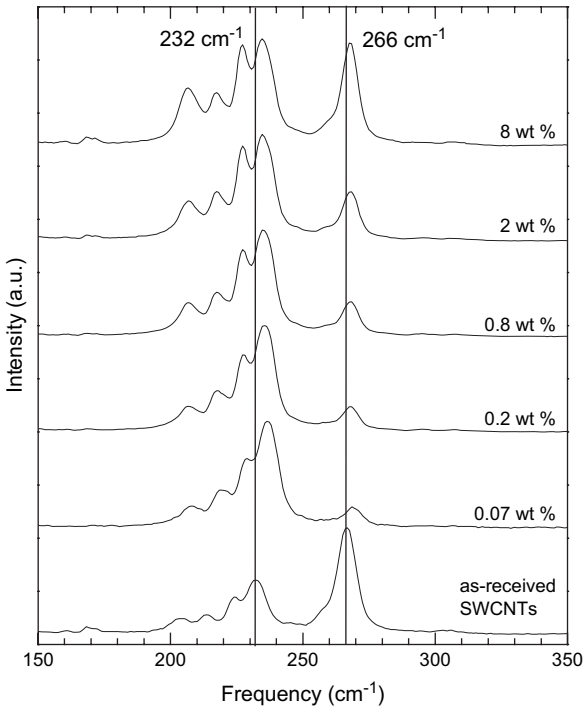

Fig. 4. Raman spectra in the radial breathing mode (RBM) region of the original SWCNTs, and 0.07, 0.2, 0.8, 2 and 8 wt% SWCNT–HDPE nanocomposites, taken with 785 nm laser excitation. Each spectrum is normalized with the highest peak intensity.

We also observe in the series of Raman spectra a shift to higher frequencies of the 266 and 232 cm^{-1} modes corresponding to the nanocomposites in reference to the "as-received" SWCNTs. These peaks shift 1.5 and 3.5 cm^{-1}, respectively. Taking as reference the work of Doorn et al. [23] and Strano et al. [24] that showed no differences in RBM frequencies for individualized and bundled unblended nanotubes, the observed shift could not be associated with intertube interactions due to a different state of SWCNT bundling. Instead, the fact that the RBM frequency is unchanged with increasing SWCNT in the nanocomposites, suggests that this shift is related to specific interactions of the nanotubes with the HDPE matrix. In reference to the as-received SWCNTs, the shift of the 232 RBM to higher values reflects nominally reduced CNT diameters. On these grounds, it is possible that the matrix exerts some compressive effect on the nanotubes, and that this effect is more pronounced in the modes associated with isolated SWCNT (the 100–250 cm^{-1} region in Fig. 4). Accordingly, modes associated with isolated nanotubes are subjected to a larger shift than for modes associated with bundles (the 266 RBM).

For SWCNT–HDPE nanocomposites, the bundle size is a characteristic of the state of SWCNT aggregation, and correlates proportionally to the intensity of the "roping" 266 cm^{-1} mode [23,24]. Note that the intensity of this RBM decreases steadily with decreasing SWCNT concentration, a signature of an effective CNT debundling, specially at the lowest concentrations. Interestingly, a small intensity "roping" RBM is present even at the lowest SWCNT concentrations studied. This feature signals the enormous difficulty to completely suppress all aggregation of SWCNT in organic solvents without surface functionalization or the use of surfactants.

It has been shown that as bundle size decreases, a steady loss in the intensity of the 266 cm^{-1} mode occurs relative to the 232 cm^{-1} mode. To probe scaling laws of the state of SWCNT aggregation given by this ratio, as a function of nanocomposite concentration, the areas of each peak were extracted after peak deconvolution of the spectral region using a non-linear regression with Lorentzian functions. As shown in Fig. 5, except for some scattering of data at the lowest concentration, the integrated intensity ratio (I_{232}/I_{266}) decreases linearly with the logarithm of the SWCNT concentration (wt%), according to the relation, $I_{232}/I_{266} = 2.98 - 2.19\log(\text{wt\%})$. For PE–CNT nanocomposites, the ratio of these two bands is clearly a very good indicator of bundle size and, thus, of the dispersion of the filler.

In addition to the RBM of interest at 266 and 232 cm^{-1}, three other RBM modes at lower frequencies are present in the as-received SWCNT and in the nanocomposites. These lower frequency modes are typical of HiPco SWCNT [24] and are associated with nanotubes of different chiralities and larger diameters [23].

The frequency of radial breathing modes (ω_{RBM}) of the two general subclasses of individual carbon nanotubes, those of the chiral and zigzag types, is known to scale proportionally to the inverse of the tube diameter ($1/d_t$) according to the equation [25]: $\omega_{RBM} = 223.5/d_t + 12.5$ for ω_{RBM} in cm^{-1} and d_t in nm. Using this relation and the observed RBM frequencies of the "as-received" SWCNT, the calculated nanotube diameters range from 1.17 nm to 0.88 nm with an averaged value of 1.05 nm. This value is in close agreement with the specifications given for HiPco SWCNT indicating that the primary structure of the SWCNTs is maintained after sonication and fabrication of the nanocomposites.

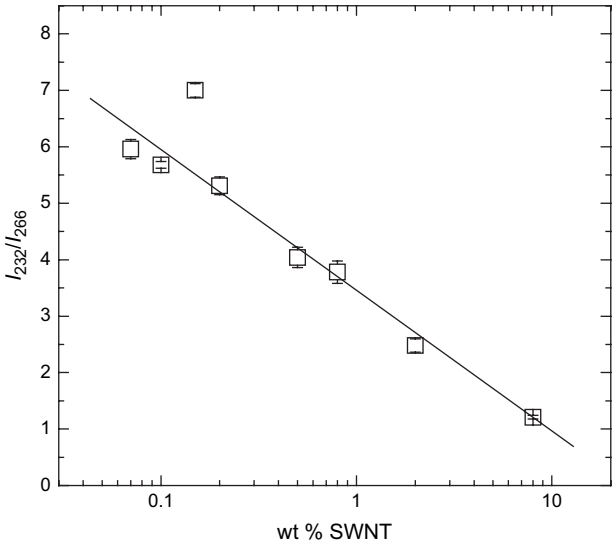

Fig. 5. Intensity ratio (I_{232}/I_{266}) of the RBM peak at ~232 cm^{-1} to the ~266 cm^{-1} peak vs. SWCNT wt% on a logarithmic scale. The error bars correspond to the standard deviation of five different measurements for each sample.

3.2. Electrical conductivity

The temperature dependent electrical resistivities ($\rho(T)$) of the nanocomposites were measured as a function of SWCNT concentration in specimens crystallized under different conditions. In the first series of measurements (Run #1), samples prepared by cooling at ~2 °C/min from the melt to room temperature (SRT) were studied, and in the second series of measurements (Run #2) samples quench-cooled to room temperature (QRT) and quench-cooled to liquid nitrogen temperature (QLN) were studied in addition to new specimens of slowly cooled samples in order to test the effect of crystallinity on conductivity. QRT and QLN samples in Run #2 developed about 20% lower crystallinity than SRT samples. Examples of the $\rho(T)$ data are shown vs. inverse temperature in Fig. 6 for Run #2 measurements. A small but systematic decrease of resistivity with increasing crystallinity is apparent from these data. In addition, we note that a positive temperature coefficient (PTC) effect [11,17] was observed when one of the samples in Fig. 6 (0.65 wt%) was raised near the melting point ($T \sim 400$ K), i.e., the resistivity of the sample increased with increasing temperature.

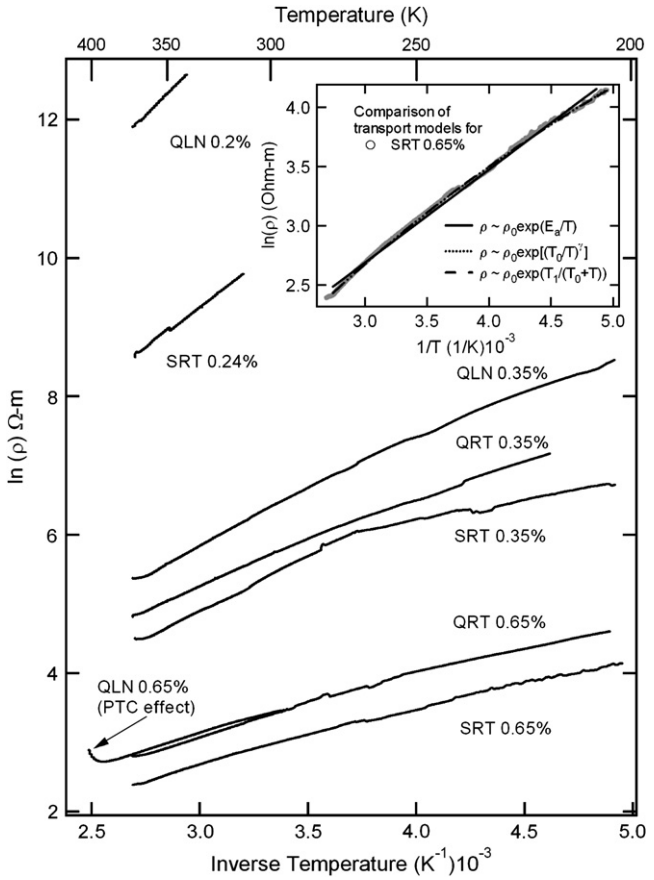

Fig. 6. Representative resistivity measurements for SWCNT–HDPE composites vs. inverse temperature. Here SRT, QRT, and QLN refer to how the samples were prepared from the melt: slow cooled to room temperature, quenched to room temperature, and quenched to liquid nitrogen temperature, respectively. The 0.2 wt% and 0.24 wt% samples only became Ohmic and measurable above room temperature, whereas for larger wt%, a broader range of temperature was accessible. In one case, a sample (QLN 0.65 wt%) was heated near the melting point to observe the PTC (positive temperature coefficient) effect. Inset: comparison of transport models (see text) for Arrhenius thermal activation ($E_a = 785.24$ K), variable range hopping ($T_0 = 4.9 \times 10^6$ K, $\gamma = 1/4$), and thermal fluctuation induced tunneling ($T_1 = 2118.5$ K, $T_0 = 173.31$ K).

Although $\rho(T)$ is thermally activated, the data do not follow a strict Arrhenius behavior $\rho(T) = \rho_0 \exp(E_a/k_B T)$ (here ρ_0 is a constant pre-factor and E_a is an activation energy) at lower temperatures. By inspection of Fig. 6 and the inset, $\ln(\rho(T))$ vs. $1/T$ is seen to be slightly sublinear where data over a large range of temperature were obtained, and two modifications of activated conductivity were considered to address this behavior. The first is the expression $\rho(T) = \rho_0 \exp[(T_0/k_B T)]^{\gamma}$, where T_0 is a characteristic barrier energy. This relation describes variable range hopping (VRH) when $\gamma = 1/4$ and Coulomb gap behavior when $\gamma = 1/2$ [26]. The second is the thermal fluctuation induced tunneling (TFIT) model, $\rho(T) = \rho_0 \exp[(T_1/(T_0 + T)]$, where T_1 and T_0 are functions of a characteristic barrier height V_0 and width w [27]. A comparison of the three different activation relationships is shown in the inset of Fig. 6 for the 0.65 wt% data, where we note that both the VRH and the TFIT models can well account for the sublinear $\ln(\rho(T))$ vs. $1/T$ behavior. (The Coulomb gap with $\gamma = 1/2$ did not fit the data as well as the VRH expression with $\gamma = 1/4$, and is not shown in the comparison). In Fig. 7 the dependence of the energy barrier terms vs. wt% for the three models is shown. In all three cases the energy barriers are seen to consistently increase very rapidly with decreasing SWCNT wt%. Since much of the resistivity data were taken over somewhat narrow temperature ranges where it is difficult to distinguish between conductivity models, we have used the simple Arrhenius fits to describe the energy barrier behavior in the discussions below.

The conductivity (σ) vs. SWCNT wt% at room temperature for all samples measured in both series is shown in Fig. 8. Normally, the linear response regions of I–V curves were used to determine the room temperature (RT) conductivity of the samples. However, for samples with less than 0.20 wt% where the RT conductivity is very low and non-Ohmic at ambient conditions, the parameters of the Arrhenius fits taken from temperature data above RT were used to estimate the RT conductivity. The electrical conductivities of slowly cooled and quenched specimens fall under the same curve in agreement with the small effect of crystallinity on electrical conductivity observed in similar HDPE and LDPE composites [13].

The data of Fig. 8 exhibit a rapid drop in the value of σ of almost four orders of magnitude over a small range in SWCNT wt% (from 0.1 to 0.3 wt%), typical of a percolation-like behavior, as depicted in the inset. Here $\ln(\sigma - \sigma_0)$ has been plotted vs. $\ln(\mathrm{wt} - \mathrm{wt}_c)$, where σ_0 is the residual conductivity signal (of order 10^{-9} S/m for wt% $\to 0$) and wt_c represents a characteristic percolation threshold for finite conductivity. By fitting the data to the percolation relationship $\sigma \propto (p - p_c)^t$ (where p is wt% in Fig. 8) we find a percolation threshold $p_c = 0.13 \pm 0.02$ wt% with a critical exponent $t \sim 3.54 \pm 1$.

The percolation threshold behavior of the SWCNT concentration is indicative of the formation of a conducting network of SWCNTs through the insulating HDPE matrix. Yet, this

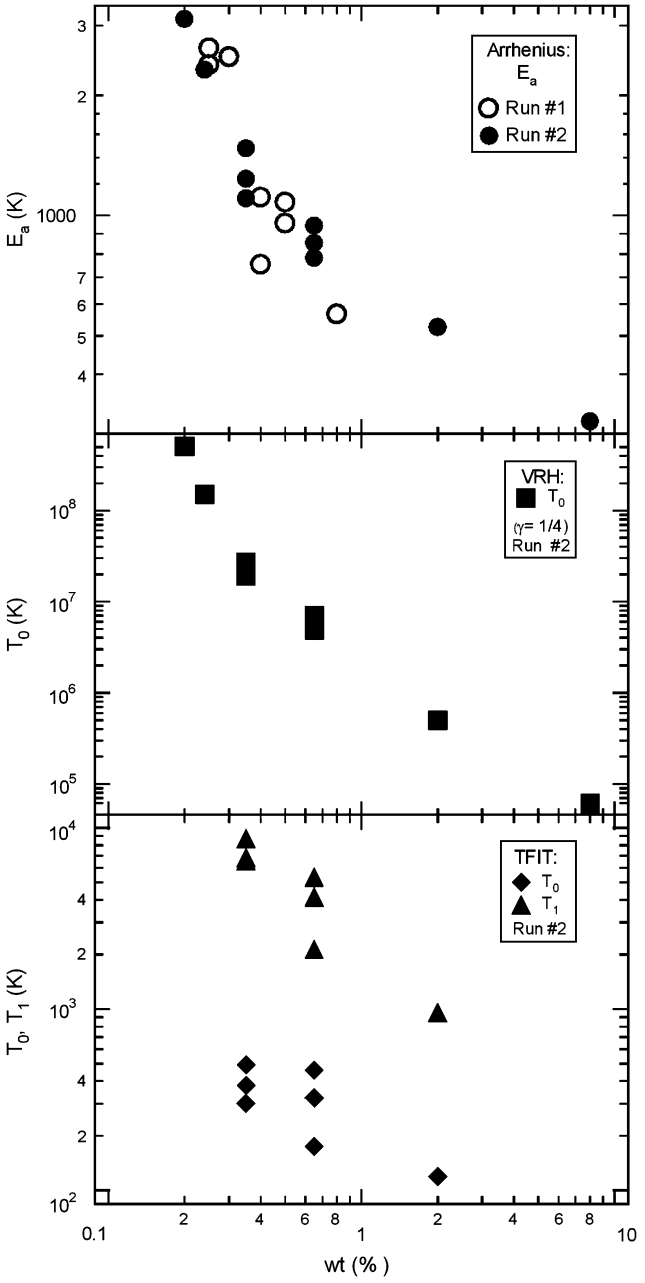

Fig. 7. Characteristic energy barrier parameters vs. wt% for Arrhenius – upper panel, variable range hopping (VRH) – middle panel, and thermal fluctuation induced tunneling (TFIT) – lower panel. The plots also include higher wt% data not shown in Fig. 6 (taken over narrower temperature ranges near room temperature). We have included only the TFIT parameters for the larger temperature range data where the two-parameter fits were more reliable.

network appears primarily built upon non-overlapping nanotubes as suggested by the SEM micrographs of Fig. 3. The values of p_c reported in the literature for different types of carbon–polyethylene composites are listed in Table 1. We find that, to our knowledge, our nanocomposites display the lowest p_c (=0.13 wt%) yet obtained for any kind of carbon–HDPE nanocomposites. Such a low critical value to achieve conductive polyethylenes attests to the effectiveness in debundling the initial SWCNTs and making use of a fast crystallization of the matrix in order to prevent further aggregation and

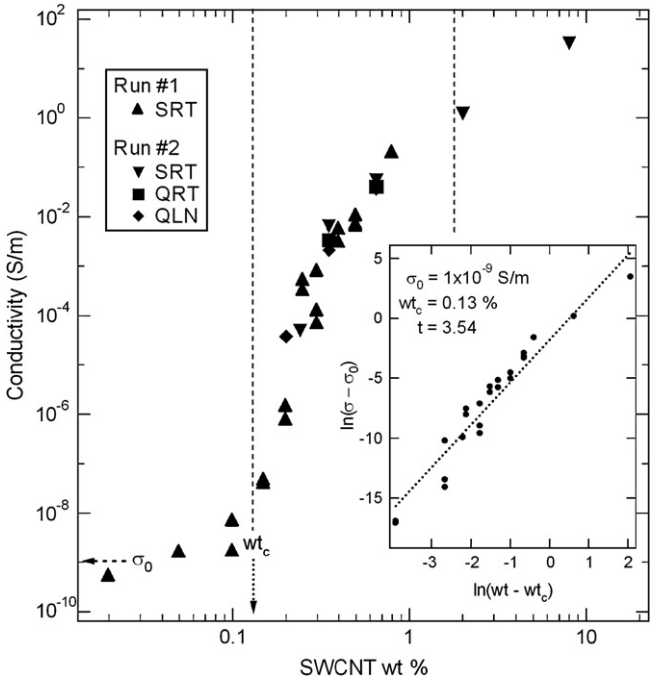

Fig. 8. Conductivity of SWCNT–HDPE composites vs. wt%. The different symbols correspond to different processing methods: slow cooled to room temperature (SRT); quench-cooled to liquid nitrogen temperature (QLN); and quench-cooled to room temperature (QRT). Dotted arrows indicate the estimated percolation threshold wt_c and the experimental limit σ_0 for low conductivity measurements (corresponding to resistances greater than ~50 GΩ). Inset: power law dependence of the conductivity corrected for the residual conductivity σ_0 on wt – wt_c, where the straight line represents the percolation relation with $wt_c = 0.13\%$ (±0.02) and an exponent $t = 3.54$ (±1). Vertical straight lines indicate calculated transitions from dilute to semi-dilute regimes (0.13 wt%) and from semi-dilute to concentrated regimes (1.71 wt%).

to maintain uniformity of SWCNT dispersion in the polymer matrix. Percolation values below 0.1 wt% have only been cited in isolated reports of nanocomposites of SWCNT [28] and MWCNT [29] with epoxy resins, and for SWCNT with polyethyleneoxide [30].

The activation and/or barrier energies (see Fig. 7) rise quickly as p_c is approached from above, indicating that the barrier for conduction is also increasing rapidly near the threshold. Although a detailed interpretation of the dependence of the activation energy near p_c is beyond the scope

Table 1
Values of percolation threshold for electrical conductivity of HDPE–carbon based composites

Composite type[a]	p_c (wt%)	Reference
UHMWPE–SWCNT	~0.6	Zhang et al. [9]
UHMWPE–MWCNT	8	Bin et al. [10a]
UHMWPE–CB	12	Jiang et al. [10b]
HDPE–MWCNT	2	He et al. [11]
HDPE–MWCNT	7.5	McNally et al. [12]
HDPE–CB	17	Hindermann-Bischoff and Ehrburger-Dolle [17]
HDPE–SWCNT	~0.45	Haggenmueller et al. [13]
HDPE–SWCNT	0.13	This work

[a] UHMWPE is ultra high molar mass polyethylene and HDPE is high density polyethylene.

of the present work, the rapid rise is consistent with a model where the nanotubes are becoming increasingly dispersed as $p \rightarrow p_c$ from high to lower SWCNT concentrations. This observation is supported by examining the relationship between the activation energy and the Raman peak ratio, as shown in Fig. 9. It is clear that there is a high correlation between the barrier energy and the degree of SWCNT separation.

Considering Doi–Edwards theory of percolation models for isotropic dispersions of rod-like particles for non-interacting rods [7], the percolation threshold is predicted to occur near the transition between the semi-dilute and concentrated regimes at a volume fraction given by $d/2L$, where d is the diameter of the rods and L the length. Nonetheless, it is found that this model does not predict well the behavior of strongly interacting CNT systems where particles may assemble as long interacting chains [8]. The latter are better represented by models that predict a critical concentration to form interconnecting long rods near the transition between a dilute and semi-dilute regime, at a volume fraction given by $3d^2/2L^2$. These latter models assume that at the critical concentration for percolation the motion of individual rods is restricted by the presence of nearby rods.

Both models give a range of concentrations where the threshold can be expected. The difficulty in applying these models to our SWCNT–HDPE nanocomposites is that we do not have a good estimation of the distribution of rod diameter and length in the nanocomposites. As a first approximation the nanotubes can be taken as homogeneous rod distributions in the HDPE matrix, with the average dimensions for lengths and diameters obtained from the histogram of Fig. 1, $d = 7.4 \pm 1.8$ nm, $L = 300 \pm 130$ nm. With these values, the calculated limiting theoretical thresholds from both models correspond to 1.2 vol% (1.71 wt%) for non-interacting rods and 0.09 vol% (0.13 wt%) for the interacting rod models. Theoretical transitions are indicated in Fig. 8.

The experimental threshold of 0.13 wt% is predicted by the model based on attractive interactions of particles that assemble to form long chains, a feature that appears parallel to the morphological observation of the distribution and geometry of SWCNT at a concentration near the percolation level (see Fig. 3). The exponent obtained from the fit of experimental data is, however, much higher than the value predicted by models of conductivity percolation for a two-dimensional ($t \sim 1$) or a three-dimensional ($t \sim 2$) system. The term t is usually conceptualized as the number of conductive connections per nanotube. While values of this exponent between 1.3 and 2 have been often reported in experimental studies of carbon nanotube composites [31–33], values higher than 3 are less common. High t values were observed in polymer composites with short carbon fibers [34] and more recently in HiPco SWCNT–epoxy composites [28]. A possible reason for this strong exponential dependence may be a result of the very rapid rise in conduction barrier energy for decreasing wt%, rather than a relatively high number of conductive connections per nanotube at the critical concentration.

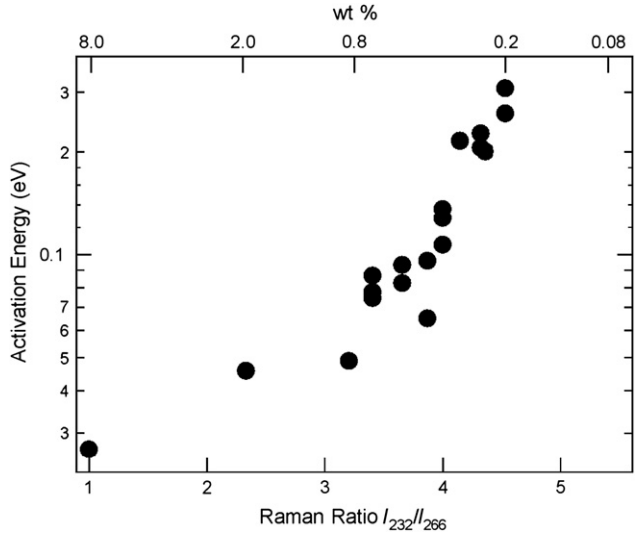

Fig. 9. Correlation of activation energy E_a (in eV) with Raman peak ratio ($I_{232}/I_{266} = 2.98-2.19$ log(wt%) from Fig. 5).

3.3. Nanocomposites' crystallization and morphology

The crystallization rate of HDPE–SWCNT nanocomposites has been found to be invariably faster than the value for the reference polyethylene [14]. The reason is the very dramatic increase in nucleation density in the melt of nanocomposites of CNT and polyethylene. We observe the same behavior in the nanocomposites studied in this work. Polarized optical micrographs (not shown) display, for the reference polyethylene, banded spherulites of ~30–50 μm diameter. In contrast, all nanocomposites, including those with the lowest concentrations in SWCNT, present smaller aggregates (1–2 μm) and greatly enhanced nucleation. On cooling from the melt at 10 °C/min, the onset and crystallization peaks of the nanocomposites are observed at 4–5 °C higher temperatures than for the reference HDPE (solvent treated). Furthermore, much faster crystallization rates of the nanocomposites are observed after isothermal crystallization as seen in the DSC exotherms of Fig. 10a and the change in peak crystallization times ($t_{1/2}$) with increasing crystallization temperature (Fig. 10b). The times required to develop half of the transformation at 124 °C are ~1 min for 2 and 8 wt% nanocomposites and increase to 2.25 min and 13.33 min for 0.05 wt% and the reference HDPE, respectively. Identifying the inverse of $t_{1/2}$ with the overall crystallization rate, the data clearly reflect the increase of the rate with SWCNT loading as a result of the nucleating activity of the nanotubes. In agreement with observations in other works [13], changes in degree of crystallinity by the presence of nanotubes are negligible. Isothermally formed crystals of the reference HDPE and of the nanocomposites, melt at the same temperature indicating that the melt-crystal transformation in both systems is taking place at the same undercooling.

Modeling the kinetics according to the Avrami formulism, Fig. 10c, gives the same $n \sim 3$ exponent for the nanocomposites (up to loads of 2 wt%) and the reference HDPE suggesting that although the nucleation density increases exponentially by the

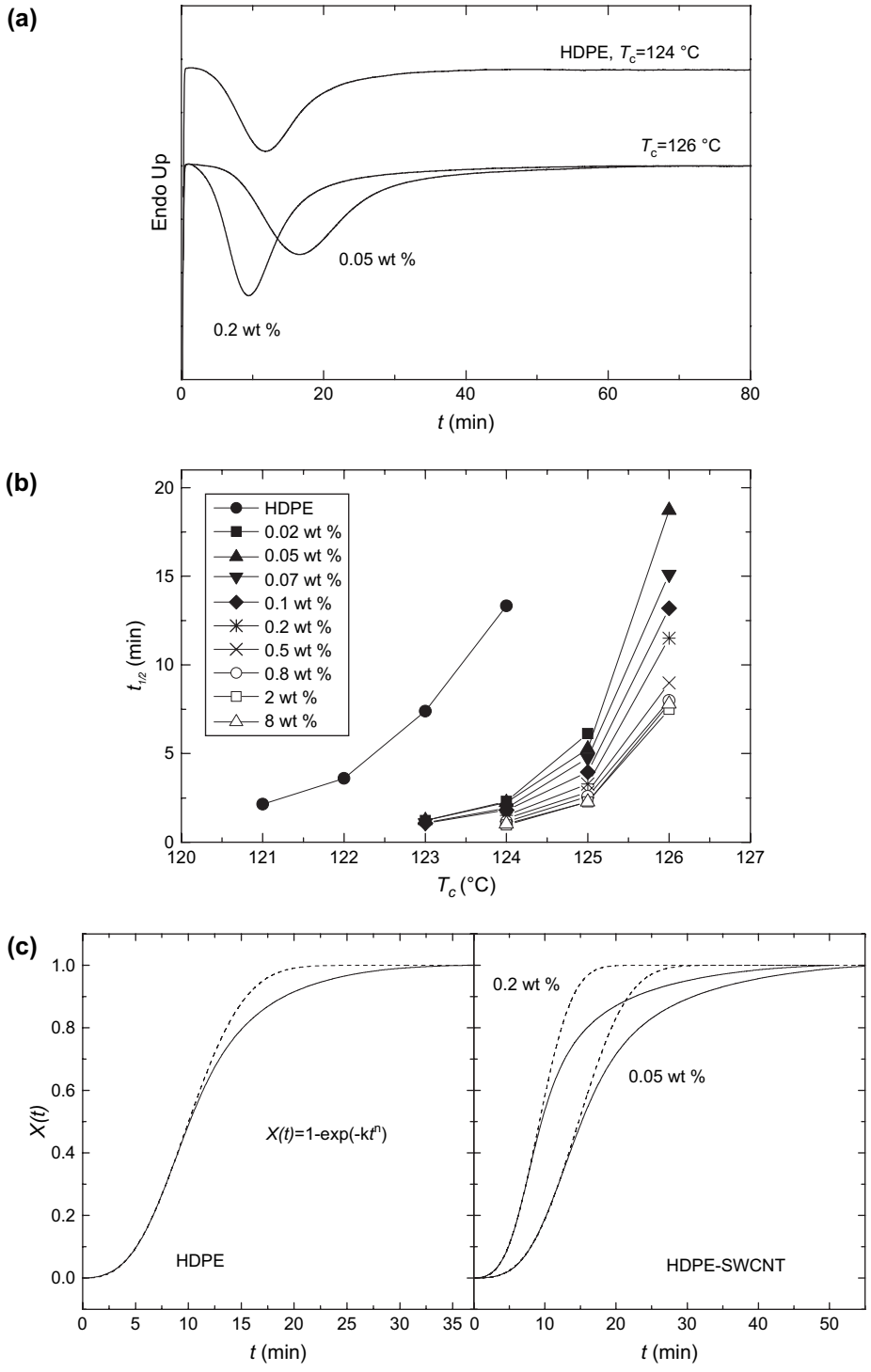

Fig. 10. (a) Isothermal crystallization exotherms for HDPE, $T_c = 124$ °C, and for 0.05 and 0.2 wt% nanocomposites, $T_c = 126$ °C. (b) Overall crystallization rate as a function of T_c for all nanocomposites. wt% loading is indicated. (c) Development of fractional content of crystals ($X(t)$) with time according to Avrami kinetics. Continuous lines are experimental data from (a), and dotted lines the best fits; HDPE, $n = 2.8$; nanocomposites 0.05 wt%, $n = 3.1$ and 0.2 wt%, $n = 2.9$.

presence of nanotubes, the growth mechanism is unchanged. The Avrami exponent of 3 is consistent with nucleation from pre-existing centers in the melt and three-dimensional growth. The postulated reduction in growth dimensionality [14] is not observed in our nanocomposites with SWCNT loads up to 2 wt%. For higher SWCNT loads, the kinetics could not be evaluated from DSC exotherms due to fast crystallization and the inability to stabilize the melt at the isothermal crystallization temperature. Hence, the change in growth mechanism, if operative, needs to be established by other methods.

Examples of a dramatic morphological change caused by the addition of SWCNT, even at the lowest concentrations

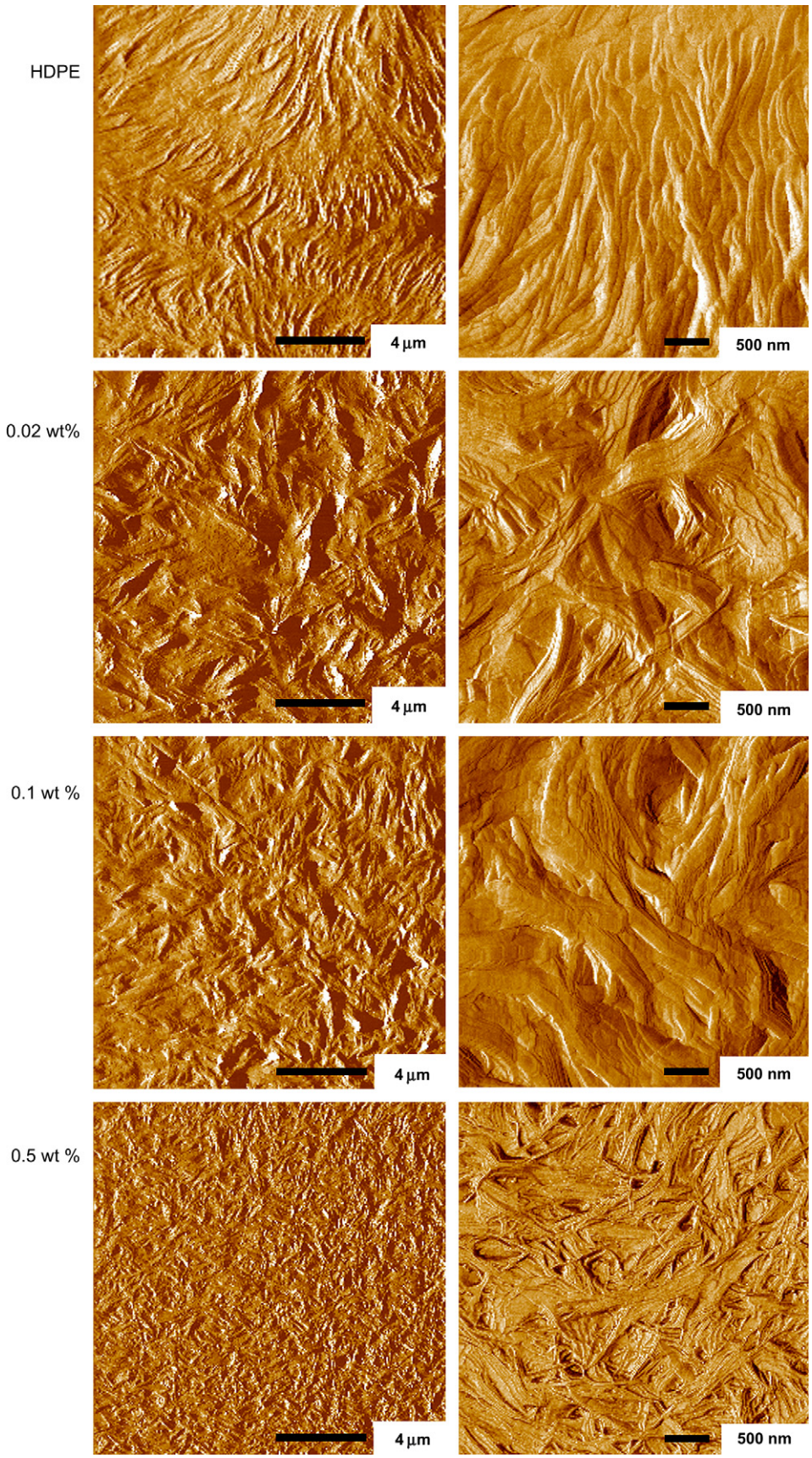

Fig. 11. AFM phase images of reference HDPE and 0.02, 0.1, and 0.5 wt% SWCNT–HDPE nanocomposites. The films were crystallized at 120 °C from the melt. Scales of $20 \times 20\ \mu m^2$ and $4 \times 4\ \mu m^2$ are shown.

(0.02 wt%) are given in the AFM images of Fig. 11. These images were obtained in thin films crystallized at 120 °C from the melt. HDPE shows periodically twisted edge-on and flat-on lamellae in banded spherulites, typical of the supermolecular morphology acquired by linear polyethylenes of a similar molar mass [35]. In contrast, the nanocomposites display a considerably larger number of non-spherulitic objects (with some axialitic character) [35] of reduced size. The AFM images project in the nanocomposites a supermolecular structure built from crystalline sheaf-like lamellae that most probably originated at the walls of the nanotubes and spread three-dimensionally from those centers. The longitudinal and lateral extensions of the lamellae are considerably reduced in the nanocomposites, in reference to those of HDPE, while in agreement with the melting behavior, the lamellar character and estimated thickness from the AFM images are basically unchanged (11.7 ± 0.8 nm).

4. Concluding remarks

Nanocomposites of HDPE–SWCNT fabricated by rapid quenching a hot solution containing polyethylene and well-dispersed SWCNT in 1,2-orthodichlorobenzene display improved electrical conductivity as the electrical percolation threshold (p_c) obtained for these nanocomposites is the lowest yet reported for polyethylene. We attribute this improvement to a good dispersion of small SWCNT bundles within the semicrystalline matrix enabled by nucleation of polyethylene crystallites on the walls of the nanotubes during fast quenching. In addition, fast crystal growth acts as a barrier to prevent nanotube clustering.

The dispersion of the nanotubes was characterized as a function of increasing SWCNT wt% in the nanocomposites using spectroscopic and imaging techniques. Upon sonication, SWCNTs do not debundle to individually separated nanotubes. At the lowest concentrations the original lump aggregates break into small separated bundles. The size of the bundle and, hence, the state of SWCNT aggregation can be followed by the intensity of the ''roping'' mode at 266 cm^{-1} by Raman spectroscopy, absent for individualized tubes. In SWCNT–HDPE nanocomposites the intensity of the ''roping'' mode increases with SWCNT concentration. In reference to the other radial breathing modes with constant intensity, the variation of the ratio I_{232}/I_{266} follows a logarithmic dependence on SWCNT wt%, given as $I_{232}/I_{266} = 2.98 - 2.19 \log(\text{wt\%})$. This relation gives a quantitative measure of the dispersion of SWCNT in a polyethylene matrix.

The room temperature activation barrier for electrical conduction rises quickly as p_c is approached due to a reduced number of nanotube contacts and increased distance between them as wt% decreases. As seen in Fig. 9, the degree of nanotube aggregation given by Raman and the barrier energy for electrical conductivity are highly correlated. Furthermore, at nanotube concentrations near the critical value for percolation, SEM images in contrast mode do not correspond to the classical geometry for electrical percolation; i.e., a network of conductive nanotubes that macroscopically overlap and connect with each other. The rapid quenching method allowed well-dispersed nanotubes in these nanocomposites, such that p_c is found at very low SWCNT concentrations (0.13 wt%). At these low wt% rod-like SWCNT bundles appear close to each other in the SEM images, yet the overlapping network geometry is observed at concentrations well above p_c (Fig. 3). At SWCNT concentrations near p_c, the high rise in activation energy and geometries of long isolated rods suggest that electron transport occurs by activated electron hopping between nanotubes that are close to each other but still electrically separate.

The nucleation activity of the nanotubes in the crystallization of polyethylene is reflected by ~6 times shorter half crystallization times of the nanocomposites. In reference to the neat HDPE, the temporal development of crystallinity of the nanocomposites follows the same three-dimensional growth geometry ($n = 3$ Avrami exponent). Moreover, the increased nucleation in the nanocomposites changes the spherulitic morphology of HDPE to axialitic-like aggregates of significantly reduced size, while the lamellar characteristics below and above p_c remain unchanged. This feature and the insensitivity of the percolation curve to changes in HDPE crystallinity suggest that electrical conductivity is dominated by dispersion and geometrical aspects of the filler and not by changes or lack thereof in the semicrystalline structure.

Acknowledgements

Funding of this work by the National Science Foundation, DMR-0503876 (R.A.) and DMR-0602859 (J.B.), is gratefully acknowledged. We also acknowledge Dr. Z. Liang and Dr. J.G. Park of the Florida Advanced Center for Composite Technologies (FAC^2T), and REU student S. Warnost for assistance with sonication, Raman spectra and with SEM images. A portion of this work was performed at the National High Magnetic Field Laboratory, which is supported by NSF Cooperative Agreement no. DMR-0084173, by the State of Florida, and by the DOE. E.S. was supported by the NHMFL/NSF REU program.

References

[1] Saito R, Dresselhaus G, Dresselhaus MS. Physical properties of carbon nanotubes. London: Imperial College Press; 1998.
[2] Moniruzzaman M, Winey KI. Macromolecules 2006;39:5194.
[3] Chen X, Yoon K, Burger C, Sics I, Fang D, Hsiao BS, et al. Macromolecules 2005;38:3883.
[4] Bahr JL, Mickelson ET, Bronikowski MJ, Smalley RE, Tour JM. Chem Commun 2001;2:193.
[5] Niyogi S, Hamon MA, Perea DE, Kang CB, Zhao B, Pal SK, et al. J Phys Chem B 2003;107:8799.
[6] Loos J, Alexeev A, Grossiord N, Koning CE, Regev O. Ultramicroscopy 2005;104:160.
[7] Doi M, Edwards SF. The theory of polymer dynamics. In: International series on monographs of physics, vol. 73. Oxford: Oxford Science Publications; 1986.
[8] Philipse AP, Wierenga AM. Langmuir 1998;14:49.
[9] Zhang Q, Lippits DR, Rastogi S. Macromolecules 2006;39:658.
[10] (a) Bin Y, Kitanaa M, Zhu D, Matsuo M. Macromolecules 2003; 36:6219;
(b) Jiang X, Bin Y, Kikyotani N, Matsuo M. Polym J 2006;38:419.

[11] He XJ, Du JH, Ying Z, Cheng HM, He XJ. Appl Phys Lett 2005; 86:062112.
[12] McNally T, Potschke P, Halley P, Murphy M, Martin D, Bell SEJ, et al. Polymer 2005;46:8222.
[13] Haggenmueller R, Guthy C, Lukes JR, Fischer JE, Winey KI. Macromolecules 2007;40:2417.
[14] Haggenmueller R, Fischer JE, Winey KI. Macromolecules 2006;39:2964.
[15] Li L, Li CY, Ni C. J Am Chem Soc 2006;128:1692.
[16] Kodjie SL, Li L, Li B, Cai W, Li CY, Keating M. J Macromol Sci Part B Phys 2006;45:231.
[17] Hindermann-Bischoff M, Ehrburger-Dolle F. Carbon 2001;39:375.
[18] Du F, Fischer JE, Winey KI. J Polym Sci Part B Polym Phys 2003; 41:3333.
[19] Flory PJ, Vrij A. J Am Chem Soc 1963;85:3548.
[20] Nikolaev P, Bronikowski MJ, Bradley RK, Rohmund F, Colbert DT, Smith KA, et al. Chem Phys Lett 1999;313:91.
[21] Chung KT, Reisner JH, Campbell ER. J Appl Phys 1983;54:6099.
[22] Dresselhaus MS, Dresselhaus G, Jorio A, Souza Filho AG, Saito R. Carbon 2002;40:2043.
[23] O'Connell MJ, Sivaram S, Doorn SK. Phys Rev B 2004;69:235415.
[24] Heller DA, Barone PW, Swanson JP, Mayhofer M, Strano MS. J Phys Chem 2004;108:6905.
[25] Dresselhaus MS, Eklund PC. Adv Phys 2000;49:705.
[26] Mott N, Davis EA. Electronic processes in non-crystalline materials. Oxford: Clarendon; 1979.
[27] Sheng P. Phys Rev B 1980;21:2180.
[28] Bryning MB, Islam MF, Kikkawa JM, Yodh AG. Adv Mater 2005; 17:1186.
[29] Sandler JKW, Kirk JE, Kinloch IA, Shaffer MSP, Windle AH. Polymer 2003;44:5893.
[30] Chatterjee T, Yurekli K, Hadjiev VG, Krishnamoorti R. Adv Funct Mater 2005;15:1832.
[31] Kim B, Lee J, Yu IJ. Appl Phys 2003;94:6724.
[32] Park C, Ounaies Z, Watson KA, Crooks RE, Smith J, Lowther SE, et al. Chem Phys Lett 2002;364:303.
[33] Ramasubramaniam R, Chen J, Liu H. Appl Phys Lett 2003;83:2928.
[34] Soares B, Gamboa K, Ferreira A, Ueti E, Camargo S. J Appl Polym Sci 1998;69:825.
[35] Bassett DC. Principles of polymer morphology. London: Cambridge University Press; 1981.